

**Effects of boundaries and point defects on energetics and dynamics of domain walls**

Ing-Shouh Hwang,\* Chung-Kai Fang, and Shih-Hsin Chang

*Institute of Physics, Academia Sinica, Nankang, Taipei, Taiwan, Republic of China 115*

(Received 25 November 2010; revised manuscript received 25 January 2011; published 20 April 2011)

Knowledge about energetics and motions of domain walls is crucial for understanding dynamics in many phase transitions and various properties of domain-wall-based materials. Through direct observation of a surface phase transition, monolayer Pb on Si(111), with a scanning tunneling microscope (STM) and careful sample preparation, the interactions of domain walls with boundaries and point defects are investigated. We observe many local dynamic phenomena near boundaries and defects such as the pinning of domain walls at constrictions and/or by point defects, dependence of transition temperatures with the domain size, enhanced structural fluctuations near boundaries and high defect density areas as well as where high defect density is artificially introduced, etc. A model based on attractive interactions of domain walls with boundaries and point defects can explain our observations qualitatively. We believe phenomena observed and explanations given for this system may be applicable for other domain-wall-rich systems, including three-dimensional systems, of nanometer size.

DOI: [10.1103/PhysRevB.83.134119](https://doi.org/10.1103/PhysRevB.83.134119)

PACS number(s): 68.35.Rh, 68.35.B-, 68.37.Ef

**I. INTRODUCTION**

A domain wall is an interface between two lattice structures or two homogeneous states. Domain walls (or grain boundaries) are commonly observed in most materials, including particles of nanometer size. Many physical properties of materials, such as structural stability, mechanical strength, and electrical and thermal conductivity, are associated with the configuration of domain walls and/or their movements. In addition, formation and migration of domain walls play a crucial role in many disordering phase transformations. Especially, it has been found that boundaries and point defects may have profound effects on energetics and dynamics of domain walls. For example, some properties of piezoelectric materials, such as hysteresis, creep, and fatigue, were attributed to the motion of domain walls and their pinning by defects during polarization switching.<sup>1</sup> It has also been demonstrated that certain responses (e.g., magnetoresistance) of magnetic devices can be engineered through the introduction of nanoconstrictions, where domain walls tend to be pinned.<sup>2,3</sup> Magnetic domain walls pinned by point defects have also been observed.<sup>4</sup> Understanding the interactions of the domain wall with boundaries and defects is of great scientific and technologic importance. It is thus highly desirable to have a systematic experimental investigation of these interactions. In particular, as the system size decreases to the nanometer scale, it can be expected that boundaries and point defects play a more important role. In this work, we will show that direct observation of a disordering structural phase transition in regions of nanometer scale can provide important information about the energetics and dynamics of domain walls and their interactions with these imperfections.

Current theoretical modeling of domain walls is mainly based on homogeneous systems.<sup>5</sup> However, real systems, especially nanometer-sized systems, are often inhomogeneous in nature due to the presence of defects and boundaries. Here we use scanning tunneling microscopy (STM) to study dynamical behaviors of domain walls in a surface phase transformation. The advantage of STM is its capability to resolve surface atomic structures and to identify atomic-scale point defects. However, domain-wall motions in many

disordering phase transitions are usually much too fast for STM imaging. In this work, through proper sample preparation and operation at appropriate temperatures, domain walls can be trapped by certain boundary and/or defect conditions, which allow us to capture domain walls and their motions at a time scale reachable by STM. Based on direct observation of local phenomena near boundaries and point defects, a kinetic picture of the energetics and dynamics of domain walls is presented. This two-dimensional (2D) system may serve as a model system to understand other domain-wall-based systems, including three-dimensional systems. It may also provide a different view to explain phenomena such as segregation of impurity atoms at dislocations or grain boundaries in many materials.<sup>6-8</sup>

The system we study, a monolayer of Pb on Si(111), exhibits a rowlike  $\sqrt{7} \times \sqrt{3}$  structure at low temperatures. It undergoes a reversible disordering transition into a  $1 \times 1$  phase near room temperature.<sup>9,10</sup> Both the  $1 \times 1$  and the low-temperature  $\sqrt{7} \times \sqrt{3}$  phases are basically a Pb monolayer on top of a bulk-terminated Si(111) substrate, and the structural transformation does not involve change in the Pb coverage.<sup>9,10</sup> We refer to the regions exhibiting either one of these two phases as the Pb-covered Si(111) regions or simply the Pb-covered regions hereafter. Previous STM studies on nearly defect-free compact Pb-covered Si(111) nanoregions suggested that this transition was caused by structural fluctuations due to the prolific creation and fast migration of domain walls at high temperatures.<sup>9,10</sup> The phase transformation involves only small displacements of Pb atoms without breaking the covalent Pb-Si bonds. At high temperatures, structural fluctuations are so fast that each Pb atom basically vibrates violently around the  $T_1$  site, resulting in the apparently ordered “ $1 \times 1$ ” structure.<sup>9</sup>

In this work, we prepare samples with different boundary and defect conditions. With continuous-time imaging of the same area at proper temperatures, the domain-wall motions associated with structural fluctuations are revealed through observation of pinning and depinning of domain walls. In addition, we deliberately introduce point defects in a low defect density region or compare the structural transformation in low

and high defect density regions to investigate the effects on the phase transition.

## II. EXPERIMENTAL

Our experiments are carried out in an ultrahigh vacuum chamber with a base pressure of  $4 \times 10^{-11}$  Torr. We start with a clean Si(111)-(7 $\times$ 7) surface.<sup>11</sup> 0.6–1.0 monolayers (1 ML =  $7.84 \times 10^{14}$  atoms/cm<sup>2</sup>) of Pb is deposited from an effusion cell onto this surface at room temperature. The sample is then annealed briefly at  $\sim 400$  °C. After annealing, we transfer the sample to the STM stage for imaging. The deposited Pb atoms have destroyed the Si(111)-(7 $\times$ 7) structure locally during the annealing and the surface forms a Si(111)-(1 $\times$ 1)-Pb (in short, 1 $\times$ 1) structure at temperatures above room temperature. This phase exhibits little corrugation in most tunneling conditions but a hexagonal 1 $\times$ 1 structure can be resolved at low biases.<sup>9,10</sup> The Pb coverage of the 1 $\times$ 1 phase has been determined to be  $\sim 1$  ML.<sup>12,13</sup> If the deposited Pb coverage is less than 1 ML, some regions of Si(111)-(7 $\times$ 7) would remain after the annealing. By controlling the Pb deposition coverage, we can prepare different kinds of samples for STM study. The sample temperature on the STM stage can be varied from room temperature down to  $\sim 60$  K and is measured with a Si sensor installed close to the sample. For atomic hydrogen exposure, H<sub>2</sub> is decomposed with a 1500 °C tungsten filament positioned  $\sim 10$  cm from the sample on the STM stage.<sup>14</sup>

We use a commercial STM (Omicron VT-STM). The STM images are usually taken at a sample bias of +2 V with a tunneling current  $\sim 0.1$ – $0.2$  nA. At this condition, we can reliably obtain good images with little tip effects on the surface dynamics. Occasionally we change to the other polarity of  $-2$  V, which allows us to identify point defects in the  $\sqrt{7} \times \sqrt{3}$  phase. To achieve atomic resolution, we can switch to low tunneling biases ( $< 1$  V), but there is a risk that the tip may crash into the surface, especially at defect sites or phase boundaries. Since we have taken many images of the monolayer Pb-covered Si(111) at various biases, we know the correspondence between the image spots taken at the +2 V sample bias and their atomic structures. Therefore, most images presented in this work are taken at biases  $\sim 2$  V.

We note that it is essential to keep the tunneling current below 0.2 nA in order not to perturb the surface structures. It has been shown that there is a chance to induce structural fluctuations in the  $\sqrt{7} \times \sqrt{3}$  phase when the tunneling current is increased to 30 nA or higher.<sup>10</sup> It was also shown that no change of the surface structure is induced by the STM tip at the tunneling current of 0.2 nA or lower.

## III. RESULTS

### A. Orientational and phase domain walls

Figure 1 shows a STM topograph of a Pb/Si(111) surface taken at 96 K. This sample is deliberately prepared to have several compact Pb-covered regions connected by narrow constrictions. Each compact region exhibits a single  $\sqrt{7} \times \sqrt{3}$  domain. Interestingly, domain walls can often be seen at the constrictions that connect neighboring compact regions. The walls X, Y, and Z belong to orientational domain walls

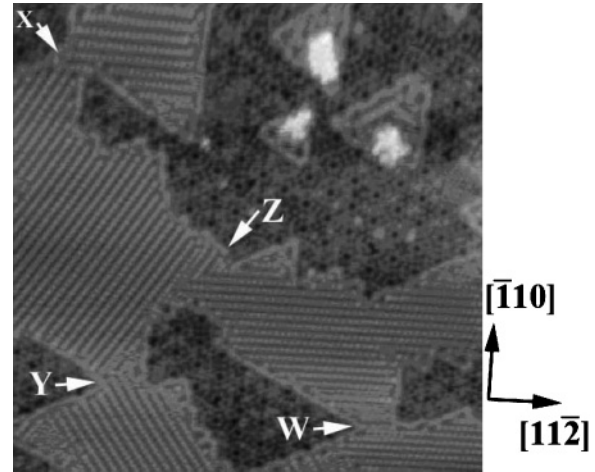


FIG. 1. STM image of compact Pb-covered regions connected by constrictions, taken at 96 K and at a sample bias of +2 V. Nearly 60% of the surface is occupied by the Pb-covered regions and the rest of the surface remains in the 7 $\times$ 7 reconstruction with a small coverage of Pb atoms on the top. The row in the  $\sqrt{7} \times \sqrt{3}$  phase is along a  $[\bar{1}\bar{1}2]$  direction. Since the Si(111) substrate has threefold symmetry, there are three different row orientations. We note that the structure of the phase domain wall *W* is not well resolved due to local fast wall motions at this temperature.

which separate domains of different orientations. Domain wall *W* belongs to the phase domain wall which separates two translationally inequivalent  $\sqrt{7} \times \sqrt{3}$  domains of the same orientation. We note that orientational and phase domain walls in Pb/Si(111)  $\sqrt{7} \times \sqrt{3}$  were also observed previously by Custance *et al.*<sup>15</sup>

Figures 2(a)–2(c) are atomic images of 60° orientational, 120° orientational, and phase domain walls, respectively. These images are taken at biases near or below 1 V. We believe that each spot seen at low biases represents a Pb atom, because the same spot can be imaged at both positive and negative biases (not shown here). Also the coverage of these spots corresponds to 1 ML of Pb atoms (1 ML =  $7.84 \times 10^{14}$  atoms/cm<sup>2</sup>), which is consistent with the coverage measurement determined by Rutherford backscattering experiments.<sup>12,13</sup> We note that the Pb atoms tend to form trimers and each trimer appears as a single protrusion for STM images taken at biases above 1 V.<sup>9,10</sup>

Figures 3(a)–3(c) illustrate typical atomic models for three types of most observed wall structures. These models are based on atom-resolved images of many domain walls obtained at low tunneling biases. The structures are basically a bulk-truncated Si(111) substrate with each first layer Si atom terminated by a Pb atom on the top. Pb atoms are either at the so-called “top, one-coordinated” sites (the *T*<sub>1</sub> sites) or slightly displaced from the *T*<sub>1</sub> site to form trimers which are centered on the so-called “hollow, three-coordinated” sites (the *H*<sub>3</sub> sites). For the models shown in Figs. 3(a) and 3(b), notice that one end of the walls often exhibits a small region of Pb trimers in the  $\sqrt{3} \times \sqrt{3}$  order. Previous STM observations of structural fluctuations featuring a sudden change in the row orientation may involve creation and fast migration of orientational domain walls [Fig. 3(a) in Ref. 9. The model shown in Fig. 3(c) is a phase domain wall, which exhibits a row structure with

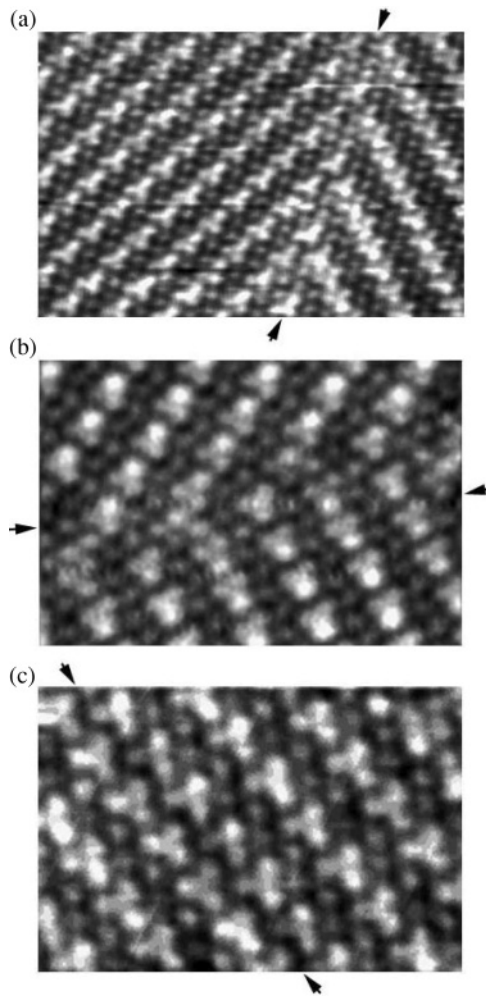


FIG. 2. Atom-resolved STM images of orientational and phase domain walls (indicated with arrows). (a) Image of a  $60^\circ$  orientational domain wall taken at the sample bias of  $-1.0$  V. (b) Image of a  $120^\circ$  orientational domain wall taken at the sample bias of  $+0.75$  V. (c) Image of a phase domain wall taken at the sample bias of  $-1.0$  V.

a local  $\sqrt{3} \times \sqrt{3}$  order along the trimer row direction. It can also be viewed as a stacking fault or a dislocation line in a  $\sqrt{7} \times \sqrt{3}$  domain. Previous STM observations of structural fluctuations featuring sudden translation in the row structure may involve creation and fast migration of the phase domain walls [Fig. 3(c) in Ref. 9]. Our STM observations indicate that the phase domain wall appears more frequently than the orientational domain walls.

The local  $\sqrt{3} \times \sqrt{3}$  structure is often present at the domain walls, thus it is another low-energy structure whose free energy is only slightly higher than that of  $\sqrt{7} \times \sqrt{3}$ . An important aspect of these models is that the Pb coverage maintains at exactly 1 ML for all of the structures in  $\sqrt{7} \times \sqrt{3}$ ,  $\sqrt{3} \times \sqrt{3}$ , and the domain walls, which is consistent with atomic images observed on this system. That means there is no Pb coverage change involved in the creation and annihilation of domain walls, in the motions of domain walls, nor in the disordering phase transition. All of these structural transformations involve only small lateral displacements of Pb atoms without breaking

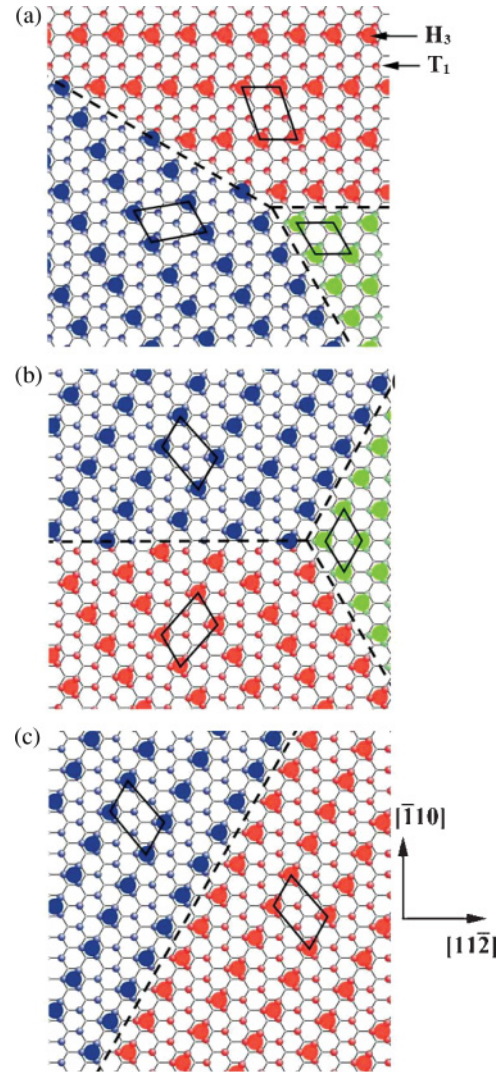


FIG. 3. (Color online) Top view model of three most observed domain walls. (a)  $60^\circ$  orientational domain wall; (b)  $120^\circ$  orientational domain wall; (c) phase domain wall. The unit cells for each  $\sqrt{7} \times \sqrt{3}$  domain are illustrated with black lines, and the unit cells of the  $\sqrt{3} \times \sqrt{3}$  are also indicated. The atomic structures are drawn based on our STM images taken at low tunneling biases. We note that the lateral displacement of Pb atoms away from the  $T_1$  sites is exaggerated somewhat. Different colors are used to represent different domains or different structures. Note that neighboring Pb atoms tend to form trimers centered on the  $H_3$  sites. In STM images taken at low biases, individual Pb atoms can be seen, but in images taken at high biases ( $>1.1$  V), each trimer appears as a single spot centered on the  $H_3$  site, which is also drawn as a colored circle in the above model. In these models, the displacements of Pb atoms in each trimer is drawn to have threefold symmetry. From the images shown in Figs. 2(a) and 2(b), however, the displacements seem not to have threefold symmetry.

the covalent Pb-Si bonds, and thus the related activation energies can be expected to be very small in the case of no strong pinning by defects or boundaries. These are consistent with the conclusions based on previous STM observations of the structural fluctuations on nearly defect-free compact Pb/Si(111) regions.<sup>9,10</sup>

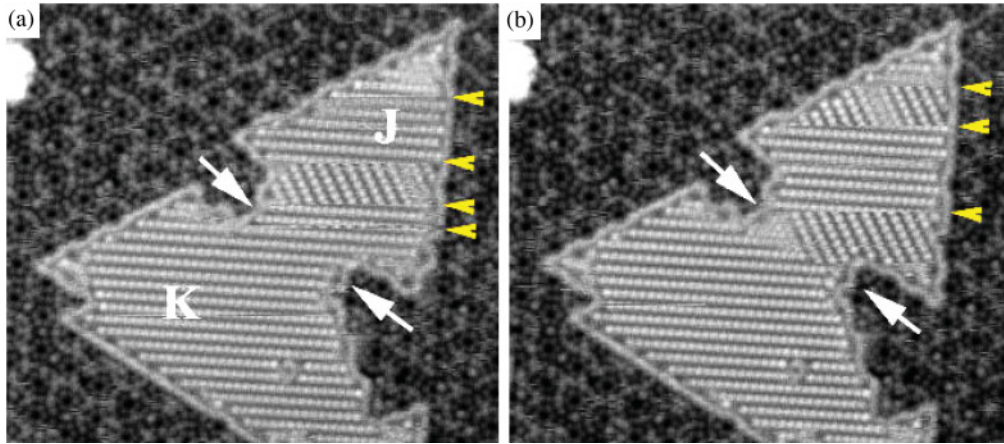


FIG. 4. (Color online) Pinning of a domain wall at a constriction. (a) and (b) show two consecutive STM images of a Pb-covered region taken at 190 K and at a sample bias of +2 V. The duration between two images is  $\sim 3$  min. The image size is  $45 \text{ nm} \times 45 \text{ nm}$ . Note that the STM images are obtained through raster scanning, so they do not represent snapshots of the surface structures. The fast scan direction of the images shown in this work is from the left to the right and the slow scan direction is from the top to the bottom. In subregion *J*, the structural changes are mainly caused by temporal fluctuations, rather than by spatial fluctuations. That means the changes are related to the change of the long-range order in the entire subregion *J*. As explained previously (Refs. 9 and 10), the short-range fluctuations are much too fast for STM imaging.

### B. Pinning of domain walls by boundaries and/or by point defects

Figures 4(a) and 4(b) show two of our consecutive STM images of a Pb-covered region taken at 190 K. This region can be separated into subregions *J* and *K* by the constriction indicated with two white arrows. In subregion *J*, structural fluctuations often appear as a sudden change in the row orientation (indicated with yellow triangles), similar to previous observations on compact nanoislands.<sup>9,10</sup> In addition, the fluctuations occur more frequently in subregion *J* than in subregion *K*. This indicates that the transition temperatures of subregions *J* and *K* are different, which is probably related to the size effects reported previously.<sup>9,10</sup> Interestingly, a  $60^\circ$  orientational domain wall appears suddenly at the constriction in Fig. 4(b) and is pinned there for at least 20 s. This pinning effect is very strong if one considers that the motions of orientational walls inside a compact region without defects (as in region *J*) are much too fast for STM imaging.

In addition to the constrictions, point defects also facilitate creation and trapping of domain walls. Figures 5(a) and 5(b) are empty-state and filled-state STM images of a  $\sqrt{7} \times \sqrt{3}$  region taken at 171 K, respectively. This structure is stable at this temperature. After exposing the surface to a small amount of atomic H, several dark point defects appear [Figs. 5(c) and 5(d)]. Meanwhile, a new  $\sqrt{7} \times \sqrt{3}$  domain,  $120^\circ$  rotated relative to the initial domain, is created at the upper-right-hand part of the Pb-covered region. The domain wall (indicated with two yellow triangles) is pinned by the H-adsorbed defects and the boundaries, and does not move within our observation time ( $\sim 6$  min). Interestingly, on the new domain at the upper-right-hand part of the image shown in Fig. 5(c), several scan lines reveal traces of fluctuations (indicated with white arrows). On similar systems after higher H exposures, more frequent structural fluctuations or even loss of the long-ranged order are often seen. An example is shown in Fig. 6.

It clearly indicates that the introduction of point defects enhances structural fluctuations and reduces the transition temperature.

Point defects alone (without boundaries) can also pin domain walls. Figure 7 shows a STM image of a Si(111) sample that is entirely covered by a Pb monolayer. A long domain wall pinned by a series of point defects is seen at 200 K. We have never imaged any immobile domain wall of similar length (or even one third of the length) with no pinning by defects. The good stability of such a long wall indicates that point defects greatly reduce the wall energy. Notice that the wall connecting neighboring defects tends to be straight. This implies that formation of a domain wall costs energy because a straight wall has a minimum length between two point defects.

### C. Heuristic picture for effects of point defects and boundaries on energetics and kinetics of domain walls

Theoretically, it is often postulated that the domain-wall energy is homogeneous. For the case of a 2D system, the wall energy is assumed to increase linearly with the wall length,<sup>5</sup> i.e.,  $E = \sigma L$ , where  $L$  is the length of the wall and  $\sigma$  is the energy per unit length. The energy zero is referred to the case of an entire ground-state domain without any wall.

Presence of atomic-scale point defects as seen in Figs. 5 and 7 does not change the wall length much, thus a reduction in wall length alone cannot explain the observed strong pinning effects. We thus propose that the point defects may serve as attractive centers for domain walls, as illustrated in Fig. 8. Here we assume that  $\sigma$  varies locally with the position of a small wall segment relative to that of point defects. The wall energy is now modified to be  $E = \int \sigma dl$ , where the line integral is over the entire wall length  $L$ . In this picture,  $\sigma$  approaches  $\sigma_\infty$  when a wall segment is extremely far away from the defect, but reduces gradually when it is close to the defect within a certain range. Domain-wall segments would

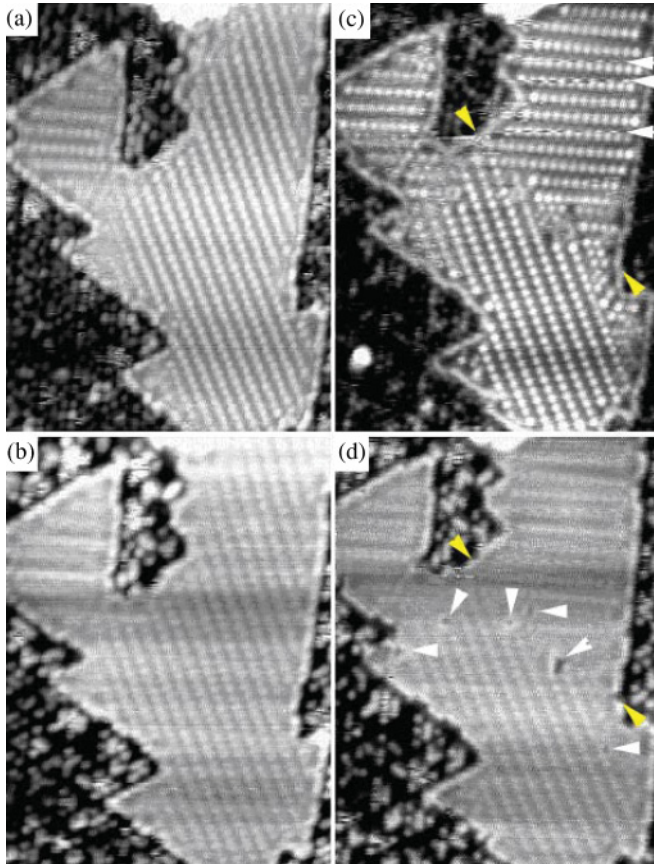


FIG. 5. (Color online) Pinning of a domain wall by point defects and boundaries. (a) and (b) are empty- and filled-state STM images taken before H exposure, respectively. (c) and (d) are empty- and filled-state STM images taken after H exposure, respectively. The sample bias for images in (a) and (c) is +2 V, and that for (b) and (d) is -2 V. The image size is 30 nm  $\times$  30 nm. We note that the H-induced defects can be discerned more easily in the filled-state images than in the empty-state images because the image contrast of the  $\sqrt{7} \times \sqrt{3}$  in the latter is much stronger than in the former. In (d), new point defects are indicated with white triangles.

experience attractive interactions from the point defect. The pinning strength,  $\sigma_0$ , occurs when a wall segment just crosses the defect. Quantitative values of  $\sigma_\infty$ ,  $\sigma_0$ , and the range of the attractive interaction vary with the type of domain walls and the type of defects. For an attractive point defect, we expect  $0 < \sigma_0 < \sigma_\infty$ . If there are several attractive point defects present locally, one can expect that they would greatly reduce the free energy of a domain wall and trap its motion if the temperature is not high enough. This may explain the observation shown in Fig. 7.

A boundary can be considered as a continuous connection of point defects and may also provide attractive potentials for domain walls. The observed strong trapping of domain walls at narrow constrictions may result from the combined effect of the shorter wall length and the attractive potentials provided by the boundaries. Similarly, formation of a short domain wall that starts at a boundary and ends at a nearby boundary does not cost much energy. Hence, new domain walls may be created constantly at boundaries, and their migrations in a small area near a boundary also do not have high-energy

barriers. This would result in the loss of the low-temperature order near boundaries at temperatures slightly below the transition temperature of the entire region, i.e., predisordering, as observed in previous STM studies.<sup>9,10</sup>

A more detailed picture about energetics of domain walls and their motions inside a compact region is described below. The blue curve in Fig. 9 illustrates a minimum potential profile for the propagation of a domain wall from a boundary on one side to another boundary on the other side. For simplicity, here we use only a one-dimensional representation of the wall position in the horizontal axis, and the compact region is illustrated with a round shape. We also assume the presence of only one wall at a time. The domain configurations are illustrated at several different wall positions. Here we would like to focus on the events that lead to the change of the long-range order, which is what can be observed in STM images. At a very low temperature, the entire compact region is mainly in a single domain, as shown in configuration  $\alpha$ . As the temperature is increased, a short domain wall which starts from a boundary and ends at a nearby boundary (configuration  $\beta$ ) can be thermally generated. The wall energy can be expected to increase if the wall propagates toward the center of the region, because the entire wall length has to increase. The wall energy reaches a maximum value when the wall moves to the center (configuration  $\gamma$ ). After the wall passes through the center, the wall energy starts to decrease because of the shorter wall length (configuration  $\delta$ ). Now the wall tends to move toward the boundaries on the other side, leading to the change of the long-range order, such as the change in the row orientation (configuration  $\epsilon$ ) or the translation of the entire row structure as seen in STM images.<sup>9,10</sup>

Clearly, the wall created at a boundary needs to overcome an energy barrier in order to move across the center of a compact region. The rate for such a center crossing becomes appreciable when the temperature is raised to the transition temperature, leading to the disordering transition. At temperatures below the transition temperature, even though the center crossing occurs rarely, the walls which are frequently created at boundaries can often move within a certain range from the boundaries. This can explain the predisordering near boundaries and an increase in the disordering area with increasing temperature reported previously.<sup>9,10</sup>

The decrease in the transition temperature with decreasing size<sup>9,10</sup> can also be understood. The red and blue curves in Fig. 9 illustrate the cases for small and large compact regions, respectively. For a smaller compact region, the maximum of the potential profile (or the energy barrier) can be expected to be lower. Thus, the disordering occurs at a lower temperature.

The dashed curve in Fig. 9 illustrates the case with the presence of several point defects, which provide pinning potentials for domain walls. If the temperature is high enough, the domain wall may be depinned from a defect and may migrate to the next pinning defect, as shown in the heuristic configurations  $\zeta$  and  $\eta$ . On the other hand, the overall energy barrier for a wall to move across the entire compact region is significantly reduced compared with the case without defects. The enhanced structural fluctuations and the decrease in the transition temperature after introduction of point defects can thus be explained.

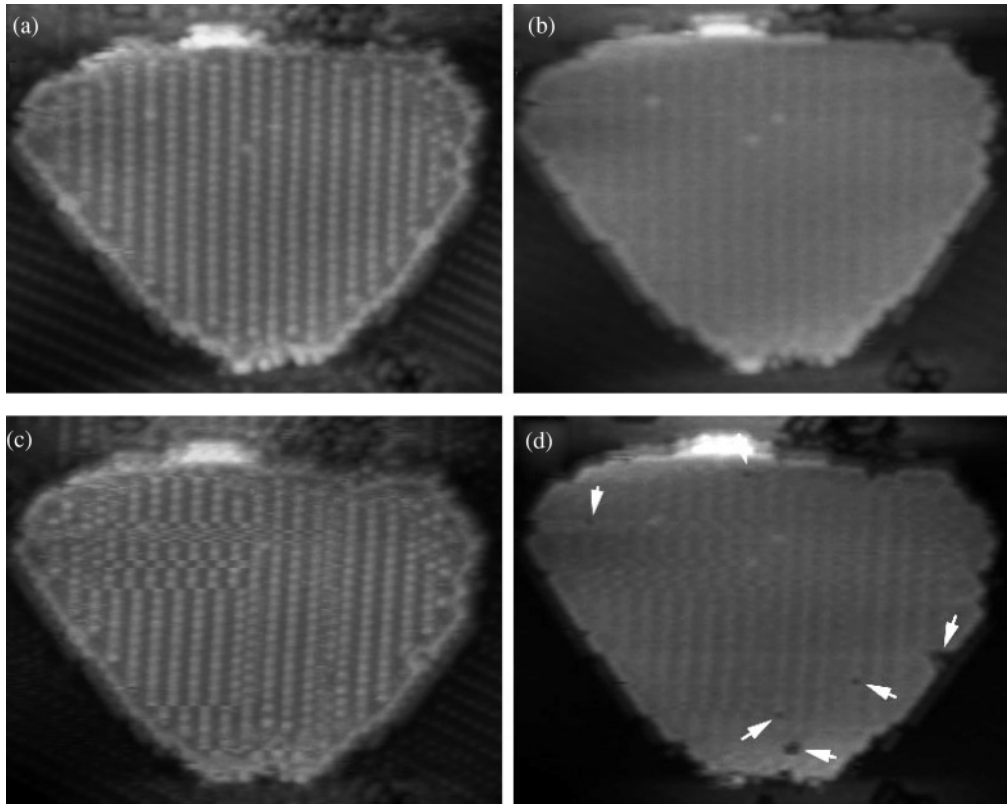


FIG. 6. STM images showing enhancement of structural fluctuations on a Pb-covered Si(111) island after the introduction of point defects. The sample temperature is 147 K. (a) and (b) are empty- and filled-state STM images taken before H exposure, respectively. (c) and (d) are empty- and filled-state STM images taken after H exposure, respectively. The sample bias for images in (a) and (c) is +2 V, and that for (b) and (d) is -2 V. The image size is 27 nm×24 nm. In (d), new point defects are indicated with white arrows.

**D. Predisordering in a high defect density area**

In a region where the local defect density is significantly higher than the average of the entire region, we can also expect predisordering to occur. This is because short domain walls connecting between neighboring defects would not have high

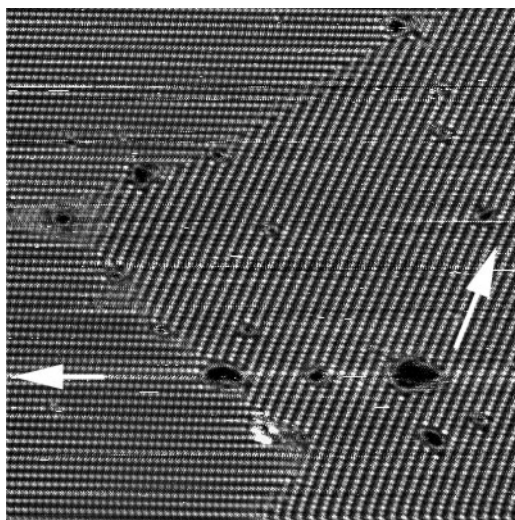


FIG. 7. STM image of a long domain wall pinned by a series of point defects, taken at 200 K and at a sample bias of +2 V. White arrows indicate the orientation of the row structures in each domain.

free energies. Domain walls can be created frequently and also migrate easily within the high defect density region at temperatures slightly below the transition temperature of the entire region. An example is shown in Fig. 10. These STM images are taken on the same area at several temperatures. Our observations indicate that the transition temperature of the entire region is ~280 K. In Fig. 10(a), there are three different domains (I, II, III) and the domain walls separating them appear to be pinned by a number of defects.<sup>16</sup>

As the temperature is increased to 256 K, structural fluctuations with sudden change in the row orientation can be observed in domain II [Fig. 10(b)]. Probably, the wall that separates domains II and III is sometimes depinned

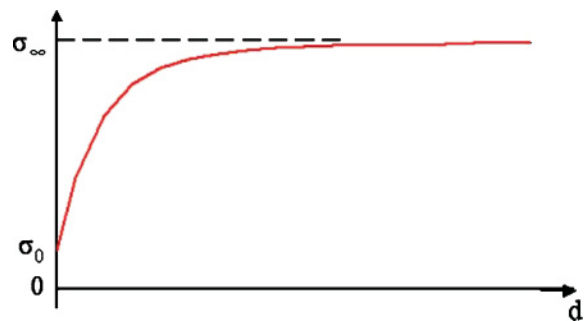


FIG. 8. (Color online) Domain-wall energy  $\sigma$  as a function of the distance from an attractive point defect.

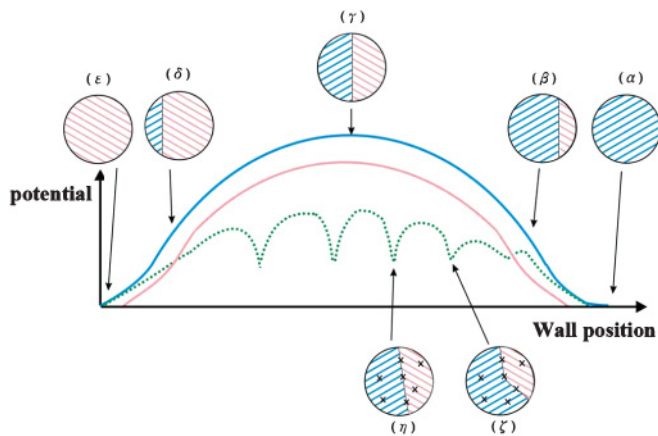


FIG. 9. (Color online) Minimum potential profile illustrated for the propagation of a domain wall originating from a boundary on one side across the center of a compact region to a boundary on the other side. Here we do not consider the activation energies for individual steps of wall motions in the potential profile, because they are negligibly small compared with the potential variations in the entire region.

from the defects and moves left out of the image, but it comes back occasionally and is pinned by the original pinning defects again. White arrows in Fig. 10(b) indicate the possible direction of the wall motions we have expected. Notice that the wall motions are much too fast for STM imaging after the wall is depinned from those defects. This reflects the amazingly long trapping time, tens of seconds as estimated from our scanning speed, once the wall is trapped by the defects. We believe that the wall sometimes moves left and gets trapped by another series of defects outside of the imaged area, but it may be depinned and moves right to the original pinning defects.

As the temperature is increased to 270 K [Fig. 10(c)], we see the formation of a disordered region (the area which does not exhibit any rowlike structure) between domains I and III. Notice that the predisordered region is now confined by a number of defects. It implies that there are high-energy barriers for the walls to move away from this high defect density region. Also, notice that domain III extends left to the entire low part of the image, because the wall that originally separates domains II and III in Fig. 10(a) is now more often trapped by the defects

to the left of the imaged area. However, the occasional streaks at the lower left-hand part of the image reveals its momentary return to the original trapping defects. The wall motions are now much faster than those seen in Fig. 10(b).

#### IV. DISCUSSION

Here we would like to summarize the effects of boundaries and point defects on the phase transition and the domain walls based on the current work and previous STM observations.<sup>9,10</sup> For the phase transition,  $\text{Pb/Si(111)}-1 \times 1 \leftrightarrow \sqrt{7} \times \sqrt{3}$ , there are three possible row orientations in the low-temperature phase due to the threefold symmetry of the substrate. For each orientation, there are five translationally inequivalent domains. For a compact region of infinite size without defects, in principle, these 15 inequivalent domains are degenerate, i.e., each domain should appear with the same probability. In real systems of nanometer sizes, the boundary and/or defect conditions may lift the degeneracy, resulting in the preferential presence of certain domains. As clearly shown in previous STM observations of structural fluctuations near the transition temperature, a certain row orientation is observed much more frequently than the other two orientations [Fig. 3(a) of Ref. 9]. In addition, STM observations also indicate that the elongated region tends to favor those domains with the long axis approximately parallel to the row orientation [Fig. 3(c) of Ref. 9]. This suggests that the region shape favors those domains with longer trimer rows. Another related observation is that predisordering near boundaries tends to occur in areas with short trimer rows [Fig. 3(a) of Ref. 9]. Clearly, the size and the shape, two important factors of the boundary conditions, have strong effects on the structural fluctuations.

For a noncompact region, the domain wall can be pinned at constrictions or by a series of point defects. Attractive potentials have been proposed to explain the observed predisordering at boundaries or in high defect density areas. We note that domain walls not terminated at any boundary or defect can also be thermally generated inside a compact region. They have higher free energies and require larger energy barriers to move across the entire regions and thus play a less important role in the change of the long-range order for nanometer-sized systems.

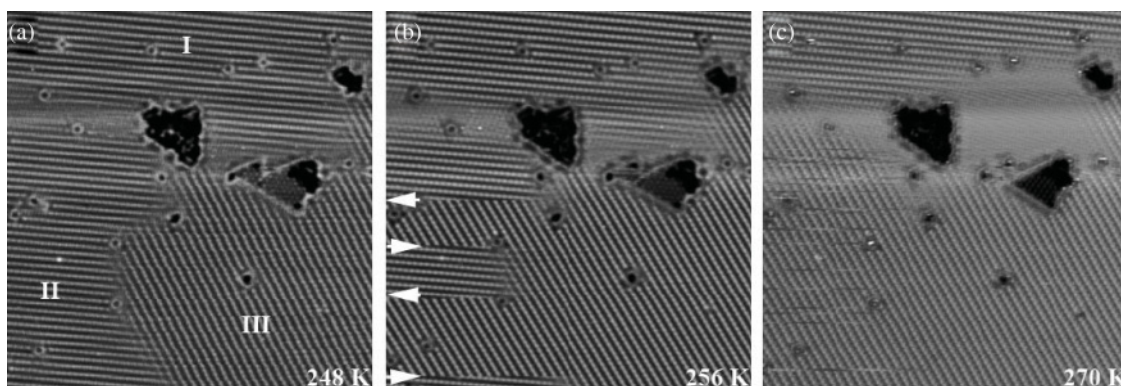


FIG. 10. (a)–(c) STM images showing predisordering phenomena in a high defect density area at three different temperatures. The temperature in each image is indicated. The slow scan direction is from top to bottom. The image size is  $44 \text{ nm} \times 44 \text{ nm}$  and the sample bias is  $+2.0 \text{ V}$ . In (c), some Pb-covered regions do not exhibit any rowlike structure because of very fast structural fluctuations in these areas.

Our new picture is complementary to the traditional thermodynamic description of disordering phase transitions caused by generation and motions of domain wall. Those theories have successfully described the associated critical phenomena and derived critical exponents for comparison with the experimental characterization of phase transitions. However, they are mainly based on homogeneous systems with an infinite size. In contrast, our kinetic picture provides a more straightforward way to describe the dynamics of domain walls at the microscopic level. Many local phenomena occurring near boundaries and point defects can be well explained.

An interesting question is whether there are defects that provide repulsive potentials. In that opposite case,  $\sigma_0 > \sigma_\infty$ , and presence of defects may stabilize the low-temperature phase, resulting in an increase in the transition temperature. A possible case is a defect-mediated phase transition of a Sn/Ge(111) system reported by Melechko *et al.*<sup>17</sup> They found that Ge substitutional defects act as nucleation centers for the low-temperature  $3 \times 3$  domain. It would be interesting to have a more detailed investigation of the dynamic behaviors in that type of system.

It has been reported that impurity atoms tend to segregate at grain boundaries (or dislocations) in many materials.<sup>6-8</sup> This might be related to attractive interactions between point defects and grain boundaries (or dislocations). A high density of impurity atoms can trap motions of grain boundaries (or dislocations). On the other hand, impurity atoms might also tend to diffuse to existing grain boundaries (or dislocations) during heat treatments because the free energy of the entire system can be reduced. This would further enhance the trapping of grain boundaries (or dislocations) by the defects. It is also known that thermomechanical processing of metals

relies on the knowledge of the migratory behaviour of grain boundaries. Therefore, microscopic understanding of energetic and dynamics of domain walls and their interaction with defects and boundaries are of great importance in materials science and technology.

## V. CONCLUSION

In this work, we propose a kinetic picture about the energetics and dynamics of domain walls based on our STM observations of many local phenomena in a surface phase transition near boundaries and point defects, such as the pinning of domain walls at constrictions and/or by defects, predisordering near boundaries and in high defect density areas, and the size effect on the transition temperature. We believe many concepts presented here can be generalized to other domain-wall-based systems, including the structural changes in three-dimensional nanoparticles. Our picture is still qualitative, therefore it would be important for further theoretical and experimental efforts to obtain the quantitative values of the detailed interactions. A quantitative understanding of the effects of point defects and boundaries would allow us to simulate real systems. Eventually it may enable our tuning the physical properties of domain-wall-rich materials and/or engineering the responses of domain-wall-based devices.

## ACKNOWLEDGMENTS

This work was supported by National Science Council of ROC (Contract No. NSC94-2120-M-001-006) and Academia Sinica.

\*Author to whom correspondence should be addressed: ishwang@phys.sinica.edu.tw

<sup>1</sup>L. He and D. Vanderbilt, *Phys. Rev. B* **68**, 134103 (2003).

<sup>2</sup>T. Ono *et al.*, *Mater. Sci. Eng. B* **84**, 126 (2001).

<sup>3</sup>K. Miyake, K. Shigeto, K. Mibu, T. Shinjo, and T. Ono, *J. Appl. Phys.* **91**, 3468 (2002).

<sup>4</sup>M. Bode, E. Y. Vedmedenko, K. von Bergmann, A. Kubetzka, P. Ferriani, S. Heinze, and R. Wiesendanger, *Nat. Mater.* **5**, 477 (2006).

<sup>5</sup>P. M. Chaikin and T.C. Lubensky, *Principles of Condensed Matter Physics* (Cambridge University Press, Cambridge, UK, 1995), Chap. 10.

<sup>6</sup>K. Seto, D. J. Larson, P. J. Warren and G. D. W. Smith, *Scr. Mater.* **40**, 1029 (1999).

<sup>7</sup>D. Blavette, E. Cadel, A. Fraczkiewicz, and A. Menand, *Science* **286**, 2317 (1999).

<sup>8</sup>D. Blavette, C. Pareige, E. Cadel, P. Auger, and B. Deconihout, *Chin. J. Phys.* **43**, 132 (2005).

<sup>9</sup>I.-S. Hwang, S.-H. Chang, C.-K. Fang, L.-J. Chen, and T. T. Tsong, *Phys. Rev. Lett.* **93**, 106101 (2004).

<sup>10</sup>I.-S. Hwang, S.-H. Chang, C.-K. Fang, L.-J. Chen, and T. T. Tsong, *Surf. Sci.* **572**, L331 (2004).

<sup>11</sup>K. Takayanagi, Y. Tanishiro, S. Takahashi, and M. Takahashi, *Surf. Sci.* **164**, 367 (1985).

<sup>12</sup>F. Xiong, E. Ganz, J.A. Golovchenko, and F. Spaepen, *Nucl. Instrum. Methods Phys. Res. B* **56-57**, 780 (1991).

<sup>13</sup>D. Nakamura, J. Yuhara, and K. Morita, *Surf. Sci.* **425**, 174 (1999).

<sup>14</sup>I.-S. Hwang, S.-H. Chang, C.-K. Fang, L.-J. Chen, and T. T. Tsong, *Phys. Rev. Lett.* **94**, 045505 (2005).

<sup>15</sup>O. Custance, J.M. Gómez-Rodríguez, A.M. Baró, L. Juré, P. Mallet, and J.-Y. Veuille, *Surf. Sci.* **482-485**, 1399 (2001).

<sup>16</sup>These wall structures are not well defined as in Fig. 2 due to some local fast wall motions between the pinning defects.

<sup>17</sup>A. V. Melechko, J. Braun, H. H. Weitering, and E. W. Plummer, *Phys. Rev. B* **61**, 2235 (2000).